**Title**

Aluminum speciation in aqueous fluids at deep crustal pressure and temperature

**Permalink**

https://escholarship.org/uc/item/9ft6h0b5

**Author**

Manning, Craig E

Peer reviewed

# Aluminum speciation in aqueous fluids at deep crustal pressure and temperature

Mainak Mookherjee [a,*], Hans Keppler [b], Craig E. Manning [c]

[a] *Department of Earth and Atmospheric Sciences, Cornell University, Ithaca, NY 14853, USA*
[b] *Bayerisches Geoinstitut, Universität Bayreuth, 95440 Bayreuth, Germany*
[c] *Department of Earth and Space Sciences, University of California Los Angeles, Los Angeles, CA 90095-1567, USA*

## Abstract

We investigated aluminum speciation in aqueous fluids in equilibrium with corundum using *in situ* Raman spectroscopy in hydrothermal diamond anvil cells to 20 kbar and 1000 °C. We have studied aluminum species in (a) pure $H_2O$, (b) 5.3 m KOH solution, and (c) 1 m KOH solution. In order to better understand the spectral features of the aqueous fluids, we used *ab initio* simulations based on density functional theory to calculate and predict the energetics and vibrational spectra for various aluminum species that are likely to be present in aqueous solutions. The Raman spectra of pure water in equilibrium with $Al_2O_3$ are devoid of any characteristic spectral features. In contrast, aqueous fluids with 5.3 m and 1 m KOH solution in equilibrium with $Al_2O_3$ show a sharp band at $\sim$620 cm$^{-1}$ which could be attributed to the $[Al(OH)_4]^{1-}$ species. The band grows in intensity with temperature along an isochore. A shoulder on the high-frequency side of this band may be due to a hydrated, charge neutral $Al(OH)_3 \cdot H_2O$ species. In the limited pressure, temperature and density explored in the present study, we do not find any evidence for the polymerization of the $[Al(OH)_4]^{1-}$ species to dimers $[(OH)_2\text{-}Al\text{-}(OH)_2\text{-}Al(OH)_2]$ or $[(OH)_3\text{-}Al\text{-}O\text{-}Al(OH)_3]^{2-}$. This is likely due to the relatively low concentration of Al in the solutions and does not rule out significant polymerization at higher pressures and temperatures. Upon cooling of Al-bearing solutions to room temperatures, Raman bands indicating the precipitation of diaspore (AlOOH) were observed in some experiments. The Raman spectra of the KOH solutions (with or without dissolved alumina) showed a sharp OH stretching band at $\sim$3614 cm$^{-1}$ and an in-plane OH bending vibration at $\sim$1068 cm$^{-1}$, likely related to an OH$^-$ ion with the oxygen atom attached to a water molecule by hydrogen bonding. A weak feature at $\sim$935 cm$^{-1}$ may be related to the out-of-plane bending vibration of the same species or to an OH species with a different environment.
© 2014 Elsevier Ltd. All rights reserved.

## 1. INTRODUCTION

Alumina is the second most abundant oxide in most crustal rocks, but its behavior in crustal metamorphic fluids has long been uncertain. While $SiO_2$ is quite soluble in $H_2O$ at metamorphic conditions (e.g., Wasserburg, 1958; Anderson and Burnham, 1967; Manning, 1994; Zotov and Keppler, 2002; Newton and Manning, 2002, 2003), $Al_2O_3$ is dramatically less so (Ragnarsdottir and Walther, 1985; Walther, 1997; Tropper and Manning, 2007). This makes it difficult to explain the common occurrence of quartz with aluminous minerals such as $Al_2SiO_5$ polymorphs in metamorphic veins (e.g., Kerrick, 1990). One possible explanation is the amphoteric nature of alumina, which leads to enhanced Al solubility in acidic and alkaline solutions (Barns et al., 1963; Azaroual et al., 1996; Wohlers and Manning, 2009). Another possible explanation is Al complexing with other components of the fluid such as salts

(Anderson and Burnham, 1967, 1983; Korzhinskiy, 1987; Sanjuan and Michard, 1987; Pascal and Anderson, 1989; Pokrovskii and Helgeson, 1995, 1997; Azaroual et al., 1996; Diakonov et al., 1996; Tagirov and Schott, 2001; Walther, 2001; Newton and Manning, 2006) or silica (Pokrovskii et al., 1996; Salvi et al., 1998; Manning, 2007).

One limitation preventing better understanding of the aqueous geochemistry of aluminum at high pressures and temperatures is fundamental uncertainty about the stabilities of various possible species. For example, it is debated whether the dominant aluminate species in alkaline solutions is $[Al(OH)_4]^{1-}$, $NaAl(OH)_4$, or $KAl(OH)_4$ (e.g., Anderson, 1995; Azaroual et al., 1996; Tagirov and Schott, 2001). In addition, it is unknown whether dissolved alumina can exist at metamorphic conditions as polymeric species. While the polymerization of silica observed at low pressure and temperature (e.g., Iler, 1979) has now been inferred to occur in metamorphic conditions as well (Zotov and Keppler, 2000, 2002; Newton and Manning, 2002), the analogous search for the large, polymerized aqueous aluminum hydroxide clusters common at surficial conditions (e.g., Casey, 2005; Casey and Rustad, 2007) has not been conducted.

To gain insight into aluminum species identities and possible polymerization at high pressure and temperature conditions, we conducted *in situ* Raman spectroscopy on aluminum-bearing solutions in hydrothermal diamond anvil cells. We carried out distinct sets of experiments by varying the chemistry and density of the aqueous fluids. The results provide new constraints on the stabilities of aluminate species at high temperature and pressure.

## 2. METHODS

### 2.1. Hydrothermal diamond anvil cell

Experiments were carried out with an externally heated Bassett-type diamond anvil cell (Bassett et al., 1993a,b; Bassett, 2003). The cell consisted of two low-fluorescence type I diamonds of 0.21 carat with 1 mm culet faces cut parallel to (100). Corrosion resistant iridium gaskets (Zotov and Keppler, 2000, 2002) with 250 µm initial thickness and 400 µm hole were used to contain the sample. Rhenium gaskets were avoided, since at high pressures and temperatures traces of rhenium dissolve into the fluid causing strong fluorescence (Zotov and Keppler, 2002). The cell was heated by coils of molybdenum wire around the tungsten carbide seats supporting the diamonds. Temperature was measured with two K-type thermocouples attached to the diamonds. The power of the upper and the lower heaters were controlled separately. This allowed the temperature of each diamond to be kept constant to ±5 °C during the heating and cooling cycles. A temperature calibration was carried out by visual observation of the melting point of NaCl inside the diamond cell. During operation, the cell was flushed with an argon (98%)–hydrogen (2%) mixture to prevent the oxidation of the diamonds and the molybdenum heaters. The maximum temperatures in the present set of experiments were limited to 1000 °C (Table 1).

The sample chamber was loaded with 1–2 pieces of synthetic corundum of high purity. The pressure was determined from the observed homogenization temperature $(T_H)$ of the vapour bubble together with the equation of state of water (Saul and Wagner, 1989). The pressure determination is based on the assumption that the sample chamber behaves as an isochoric system and that the equation of state of the fluid is similar to that of pure water (Bassett et al., 1993b). While the latter assumption is certainly valid for the $Al_2O_3$–$H_2O$ system, systematic deviations from the equation of state are possible for the KOH solutions and uncertainties in estimated pressures may reach 10–20%. Moreover, in the KOH-bearing systems, alumina solubility at high temperature is so large that precipitation of AlOOH may occur upon cooling (see below). This precluded repeated pressure–temperature cycling of the cell before the Raman measurement, so that significant deformation of

Table 1
Experimental conditions, chemical composition of fluids in equilibrium with corundum crystal, homogenization temperatures upon heating and cooling, and maximum temperature explored in each experiments.

| Exp name # | Chemical System | Cell used | Heating | | Cooling | | $T_{max}$ (°C) |
|---|---|---|---|---|---|---|---|
| | | | $T_H$ (°C) | $\rho$ (g/cm$^3$) | $T_H$ (°C) | $\rho$ (g/cm$^3$) | |
| H | Pure $H_2O$ | HDAC-2 | 45.0 | 0.99 | 177.0 | 0.89 | 809.0 |
| KH5 | 5.3 m KOH | HDAC-2 | 40.0 | 0.99 | 370.0 | 0.45 | 812.7 |
| ALH-I | $Al_2O_3$ + pure $H_2O$ | HDAC-3 | – | 1.09[§] | – | 1.09[§] | 718.4 |
| ALH-II | $Al_2O_3$ + pure $H_2O$ | HDAC-3 | – | 1.08[§] | 300.0 | 0.71 | 1000.0 |
| ALKH5-I[*] | $Al_2O_3$ + 5.3 m KOH | HDAC-3 | 237.0 | 0.79 | – | – | 801.5 |
| ALKH5-II | $Al_2O_3$ + 5.3 m KOH | HDAC-3 | 166.5 | 0.90 | 230.0 | 0.83 | 811.9 |
| ALKH5-III[*] | $Al_2O_3$ + 5.3 m KOH | HDAC-3 | – | 1.01 | – | – | 800.3 |
| ALKH5-IV[*] | $Al_2O_3$ + 5.3 m KOH | HDAC-3 | – | 1.00[§] | – | – | 614.8 |
| ALKH1-I[*] | $Al_2O_3$ + 1 m KOH | HDAC-2 | – | –[∞] | – | – | – |
| ALKH1-II[*] | $Al_2O_3$ + 1 m KOH | HDAC-2 | – | 1.24[§] | – | 1.24[§] | 200.0 |
| ALKH1-III[*] | $Al_2O_3$ + 1 m KOH | HDAC-2 | – | 1.24[§] | – | – | 772.1 |
| ALKH1-IV | $Al_2O_3$ + 1 m KOH | HDAC-3 | 25.0 | 1.00 | 250.0 | 0.79 | 714.4 |

$\rho$ are equivalent densities for pure water as determined from the observed homogenization temperatures; the actual densities of the KOH solutions are higher.
[*] Data were not collected during cooling path, either due to leak, gasket collapse, or dissolution of crystal.
[§] Initial density is based on ruby fluorescence at ambient condition.
[∞] Trouble with heater and thermocouple wires.

the cell may have occurred during heating, as indicated by major changes in homogenization temperature after the experiment. In such cases, measurements were carried out during the cooling path and it was assumed that the cell had remained isochoric during cooling (i.e., all deformation had happened during heating). For the experiments with initial fluid density >1 g/cm$^3$, i.e., without a vapor bubble at room temperature conditions, the initial density is determined by comparing the shifts in the fluorescence spectra of a ruby chip at ambient condition and the piece of corundum within the HDAC. The initial density is calculated by converting the $\Delta v$ to pressure based on existing calibration on variation of ruby fluorescence under compression (Mao et al., 1986). The estimated error in the determination of the pressure is of the order of ±1.0 kbar (Wei et al., 2011)

and the resulting error in the estimation of the fluid density is of the order of ±0.3 g/cm$^3$.

## 2.2. In-situ Raman spectroscopy

Raman spectra were collected with a Horiba Jobin-Yvon Labram HR 800 UV spectrometer using the 514 nm line of an argon laser at 2 Watt output power for excitation. The spectrometer was equipped with a 1800 gr/mm grating and a Peltier-cooled CCD detector. Measurements were made in backscattering geometry with an Olympus microscope using an objective SLMP LAN N 50 × (numerical aperture = 0.35) in conjunction with confocal optics. In order to obtain a reasonable signal to noise ratio, the measuring times were relatively long (2 accumulations of 60 s per

Table 2
Energetics and main vibrational modes for aluminum species in aqueous solutions calculated using density functional theory with B3YLP basis set. All the calculations were done in the gas phase.

| Species | Energy (a.u.) | Frequency (activity) [cm$^{-1}$ (A$^4$/AMU)] | | | | | | |
|---|---|---|---|---|---|---|---|---|
| | | 0–399 | 400–499 | 500–599 | 600–699 | 700–799 | 800–899 | 900–1099 |
| $(OH)^{1-}$ | −75.80 | | | | | | | |
| $H_2O$ | −76.43 | | | | | | | |
| $H_2O\text{-}OH^{1-}$ | −152.29 | 197.1 (1.3) | | 505.5 (4.6) | | | | 1028.1 (28.1) |
| | | 286.8 (8.3) | | 590.1 (4.3) | | | | |
| *Al-monomers* | | | | | | | | |
| $Al^{3+}\text{-}6H_2O$ | −700.82 | 347.8 (0.6) | 446.2 (4.9) | 538.9 (2.5) | | | | |
| | | | | 543.3 (2.5) | | | | |
| | | | | 543.7 (2.5) | | | | |
| $Al(OH)_3$ | −470.10 | 215.9 (1.1) | | | 621.6 (5.6) | | | 923.5 (1.7) |
| | | 217.6 (1.1) | | | 690.4 (12.0) | | | 923.7 (1.6) |
| $Al(OH)_3\cdot H_2O$ | −546.57 | 209.1 (1.3) | 428.1 (0.8) | | 604.4 (5.8) | 710.6 (2.7) | 861.6 (0.9) | |
| | | | | | 635.8 (1.2) | | 867.6 (1.2) | |
| | | | | | 658.2 (5.5) | | | |
| | | | | | 687.6 (2.2) | | | |
| $[Al(OH)_4]^{1-}$ | −546.05 | 355.3 (1.0) | | 586.1 (11.8) | 684.9 (2.3) | | | |
| | | | | | 690.6 (1.1) | | | |
| | | | | | 690.7 (1.1) | | | |
| $K[Al(OH)_4]$ | −1145.96 | 244.7 (1.1) | | 591.0 (10.3) | | 757.1 (1.4) | | |
| | | | | | | 770.3 (1.2) | | |
| *Al-dimers* | | | | | | | | |
| $[(OH)_3\text{-}Al\text{-}O\text{-}Al(OH)_3]^{2-}$ | −1015.55 | 232.7 (1.2) | | 500.7 (15.6) | 626.1 (1.7) | | | 932.2 (2.1) |
| | | 237.0 (1.1) | | 572.8 (2.9) | 640.1 (1.9) | | | 953.4 (1.2) |
| | | 368.9 (2.6) | | | 660.0 (1.0) | | | |
| | | | | | 671.6 (1.8) | | | |
| | | | | | 679.4 (2.1) | | | |
| $[(OH)_2\text{-}Al\text{-}(OH)_2\text{-}Al(OH)_2]$ | −940.29 | 88.94 (1.5) | 411.5 (2.8) | | 601.3 (1.4) | | 821.3 (8.7) | |
| | | 185.2 (1.1) | | | 633.4 (9.2) | | 871.7 (3.4) | |
| | | 348.9 (1.4) | | | 649.6 (2.7) | | | |
| *Al-trimer* | | | | | | | | |
| $[\{\text{-}(OH)_2\text{-}Al\text{-}O\text{-}\}_3]$ | −1408.49 | 114.5 (1.2) | | 504.2 (5.1) | 612.8 (1.6) | | 814.1 (6.0) | |
| | | 223.1 (1.6) | | 535.4 (1.7) | 628.9 (1.9) | | 830.5 (8.4) | |
| | | 244.4 (3.7) | | 543.8 (1.3) | 647.2 (4.0) | | 833.8 (3.9) | |
| | | 291.4 (1.6) | | 566.5 (3.3) | 651.3 (3.6) | | 839.6 (4.1) | |
| | | 308.3 (2.0) | | 577.7 (2.4) | | | 844.3 (10.6) | |
| | | 352.0 (1.8) | | | | | 882.6 (3.1) | |
| | | 373.6 (9.5) | | | | | 888.1 (2.5) | |
| | | 382.2 (3.6) | | | | | | |
| | | 389.9 (10.4) | | | | | | |

spectral window). A confocal aperture of 300 μm was used to limit the sampling volume; spectral resolution was 2.5 cm$^{-1}$.

The blackbody contribution measured at high temperatures of 800 °C is only few percent of the Raman signal from the solution and is nearly independent of frequency over the spectral window of the present study. Hence, no correction for the black body radiation was made.

The Horiba Jobin-Yvon Labram HR Raman spectrometer has confocal microscopy capabilities; however, the spectra collected often contained minor contributions from diamond fluorescence. This is because the signal collected from the volume of aqueous fluid travels through the upper diamond. We selected diamonds with minimum fluorescence. In order to remove minor features related to diamond fluorescence, we corrected the spectra of the solution by subtracting the spectrum of the upper diamond measured at the same temperature.

### 2.3. *Ab initio* simulations

In order to gain insights into the various aluminate species, the geometry optimizations of the species were performed with the Becke's three-parameter combination of Hartee-Fock and gradient-corrected density functional exchange combined with the non local correlational functional of Lee-Yang-Parr (B3LYP) (Lee et al., 1988; Becke, 1993). The B3LYP hybrid functional has been quite reliable in optimizing the geometry and prediction of vibrational spectrum of the alumino-silicate species (Gale et al., 1998; Tossell, 1999; Mibe et al., 2008). All the calculations were performed using the 6-31G$^{**}$(d, p), a triple split valence basis sets with polarized p and d orbitals and diffuse functions ($^{**}$) (Hehre et al., 1986) as implemented in

Gaussian 09 (Frisch et al., 2009). We considered several species including

(a) *Monomers* – (i) $Al(H_2O)_6^{3+}$, where $Al^{3+}$ is surrounded by six water molecule in octahedral configuration, (ii) $Al(OH)_3$ with a planar trigonal configuration; (iii) $Al(OH)_3 \cdot H_2O$ with a distorted tetrahedral arrangement and overall neutral charge, (iv) $[Al(OH)_4]^{1-}$ with the $Al^{3+}$ ion in the center of a tetrahedron formed by $OH^-$ ions, and (v) $K[Al(OH)_4]$, where a potassium ion is attached to the tetrahedral $[Al(OH)_4]^{1-}$ unit, thus rendering it charge neutral.

(b) *Dimers* and *trimers* – (vi) $[(OH)_3-Al-O-Al(OH)_3]^{2-}$ with alumina tetrahedral units sharing a bridging oxygen atom and (vii) $[(OH)_2-Al-(OH)_2-Al-(OH)_2]$ with edge-sharing alumina tetrahedral units with two fully protonated bridging oxygen atoms; (viii) alumina tetrahedral units forming a cyclic trimer $[\{-Al(OH)_2-O-\}_3]$, (ix) interaction between $H_2O$ molecules and excess $OH^{1-}$ arising due to addition of KOH into the aqueous solution (Table 2, Fig. 1).

All calculations for energetics and vibrational frequency were done in the gas-phase and as a result, the theoretically predicted vibrational frequencies for the gas-phase molecule are often lower than the experimentally observed frequencies (Pople et al., 1993). Hence, for the individual aluminate species, the theoretically predicted vibrational frequencies need to be multiplied with a scaling factor of 1.04 as noted in previous studies on alumino-silicate clusters (Mibe et al., 2008). Hence for instance, our predicted vibrational frequency for $K[Al(OH)_4]$ will be 615 cm$^{-1}$, i.e., $1.04 \times 591$ cm$^{-1}$ (Table 2).
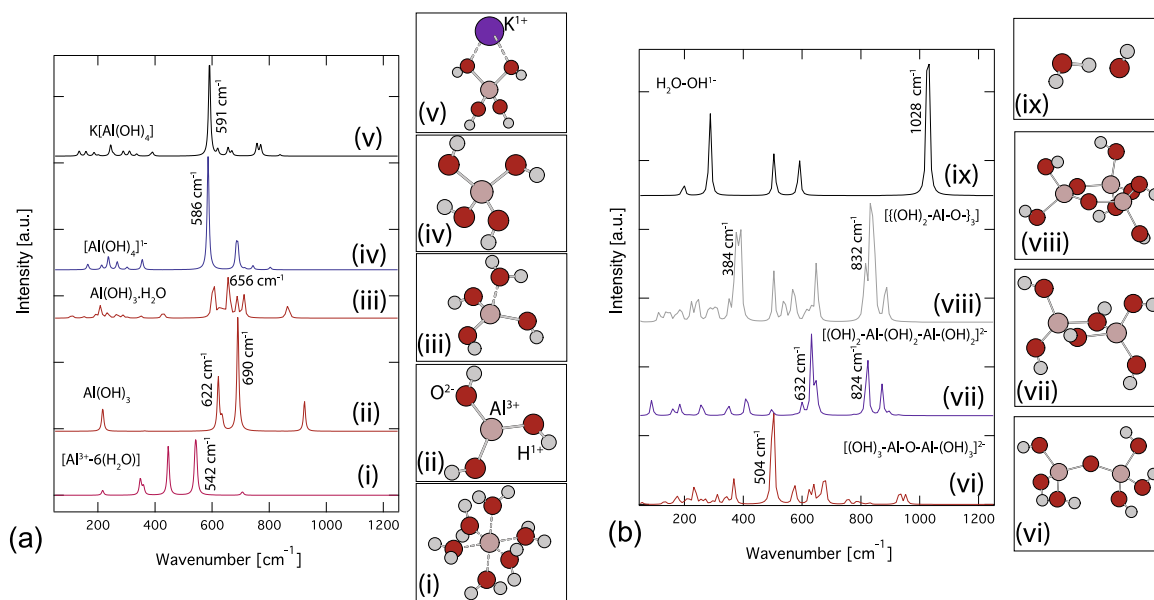


Fig. 1. Raman spectra for aluminum species in aqueous fluids calculated using density functional theory, (a) monomers and (b) dimers, trimers, and $H_2O-OH^{1-}$ interactions. Also shown are the optimized geometries of the aluminum species (i) $Al^{3+}-6H_2O$, (ii) $Al(OH)_3$, (iii) $Al(OH)_3 \cdot H_2O$, (iv) $[Al(OH)_4]^{1-}$, (v) $K[Al(OH)_4]$, (vi) $[(OH)_3-Al-O-Al(OH)_3]^{2-}$, (vii) $[(OH)_2-Al-(OH)_2-Al-(OH)_2]$, (viii) $[\{-(OH)_2-Al-O-\}_3]$, and (ix) $H_2O-OH^{1-}$.
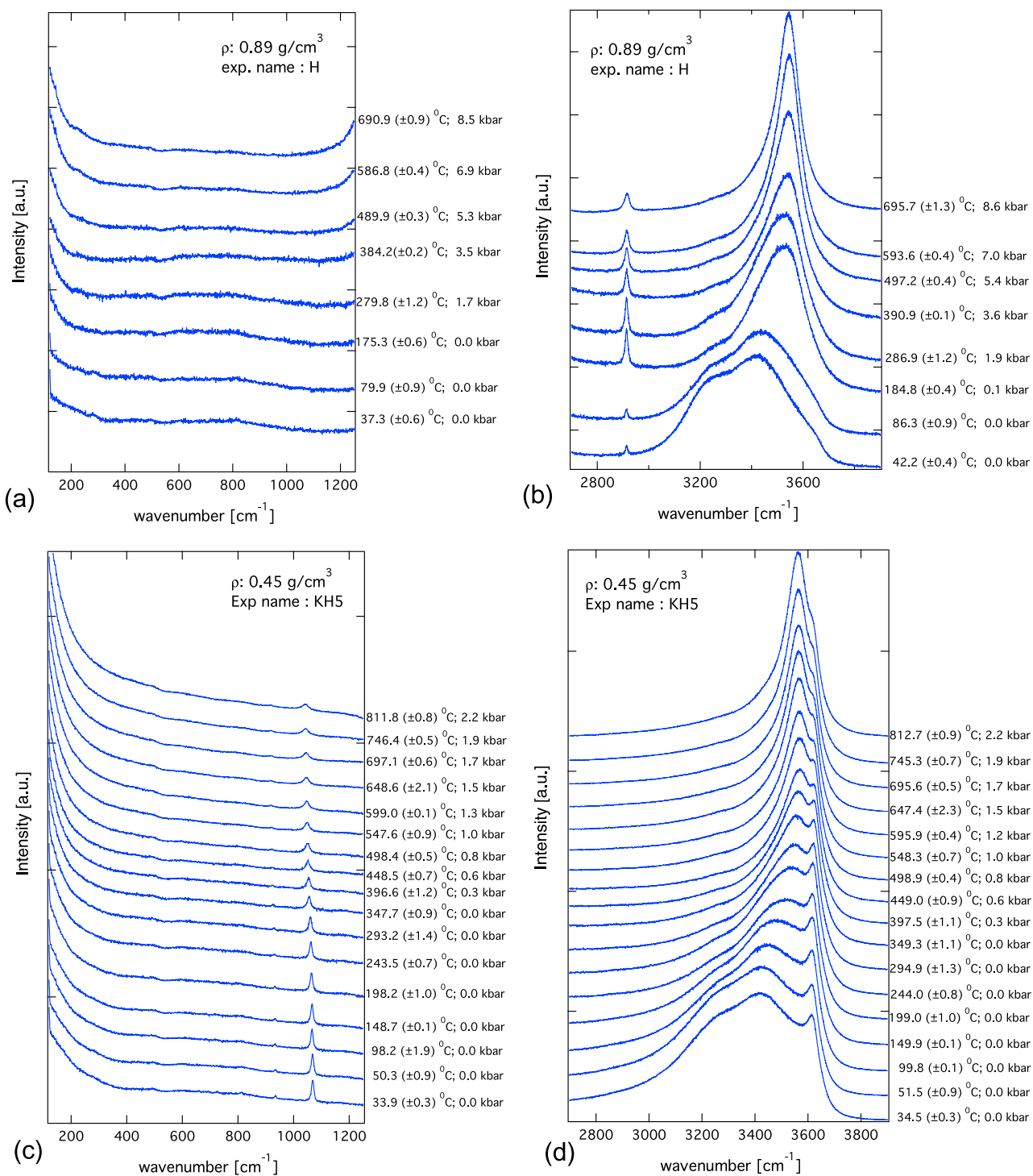
Fig. 2. Raman spectra of pure $H_2O$ and 5.3 m KOH aqueous solution as measured along an isochore: (a) The 100–1200 cm$^{-1}$ region for the pure water is devoid of any vibrational features, (b) the 2800–4000 cm$^{-1}$ region for the pure water is characterized by three distinct bands at 3256 cm$^{-1}$, 3452 cm$^{-1}$, and 3606 cm$^{-1}$. In addition, there are features at $\sim$ 2913 cm$^{-1}$ due to methane produced by interaction of the diamond and water at high temperatures, (c) the 100–1200 cm$^{-1}$ region for the 5.3 m KOH solution contains a feature at $\sim$1068 cm$^{-1}$ due to the $\delta$(OH) mode, and (d) the 2800–4000 cm$^{-1}$ region for the 5.3 m KOH solution contains intramolecular water bands at 3348, 3542, and 3564 cm$^{-1}$ and a sharp feature at 3614 cm$^{-1}$ probably related to the stretching vibration of the dissolved OH$^{1-}$ ion.
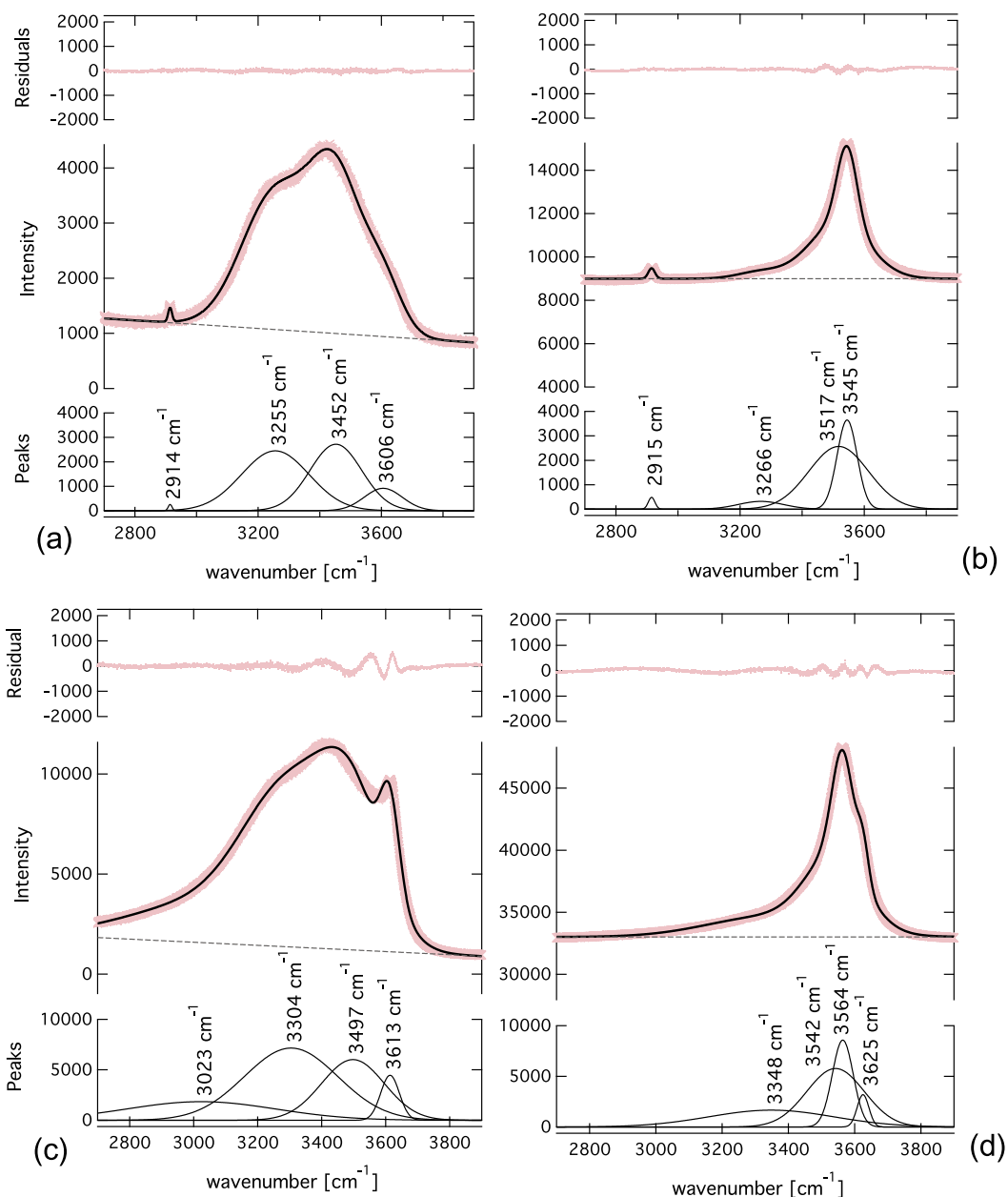
Fig. 3. Deconvolution of the 2700 to 4000 cm$^{-1}$ region of the Raman spectrum of pure H$_2$O (a, b) and of 5.3 m KOH solution (c, d). There are three panels, top indicates the residual (pink dots), the middle panel indicates the data (pink crosses), the fit (black line), and the baseline (dashed line) and the lower panel shows the deconvoluted peaks. The bands for pure water occur at (a) 3255 cm$^{-1}$, 3452 cm$^{-1}$, and 3606 cm$^{-1}$ at 42 °C, 0 kbar, and the bands shift to (b) 3266 cm$^{-1}$, 3517 cm$^{-1}$, and 3545 cm$^{-1}$ at 696 °C, 8.6 kbar. We also observe the band at 2914 cm$^{-1}$ due to methane produced by the interaction of diamond and pure water upon heating. The band may persist even when the hydrothermal diamond anvil cell is cooled. The spectral region of 2800–4000 cm$^{-1}$ for the 5.3 m KOH aqueous solution, consists of distinct bands at (c) 3023 cm$^{-1}$, 3304 cm$^{-1}$, 3497 cm$^{-1}$, and 3613 cm$^{-1}$ at 34.5 °C, 0 kbar; upon heating along an isochore (d), the bands shift to 3348 cm$^{-1}$, 3542 cm$^{-1}$, 3564 cm$^{-1}$, and 3625 cm$^{-1}$ at 812.7 °C, 2.2 kbar system. (For interpretation of the references to color in this figure legend, the reader is referred to the web version of this article.)

## 3. RESULTS

### 3.1. Blank experiments

Reference Raman spectra of Al-free systems were collected for (i) pure water and (ii) 5.3 m KOH solution. It has been noted that the rhenium gaskets used for hydro-thermal diamond anvil cell experiment often reacts with the aqueous fluids (Chellappa et al., 2009). However, we have used iridium gaskets to avoid strong fluorescence (Zotov and Keppler, 2002) and we do not observe features in the Raman spectra that could be attributed to the formation of iridium oxides. Hence, there is no evidence of reaction of the iridium gasket with the aqueous fluid
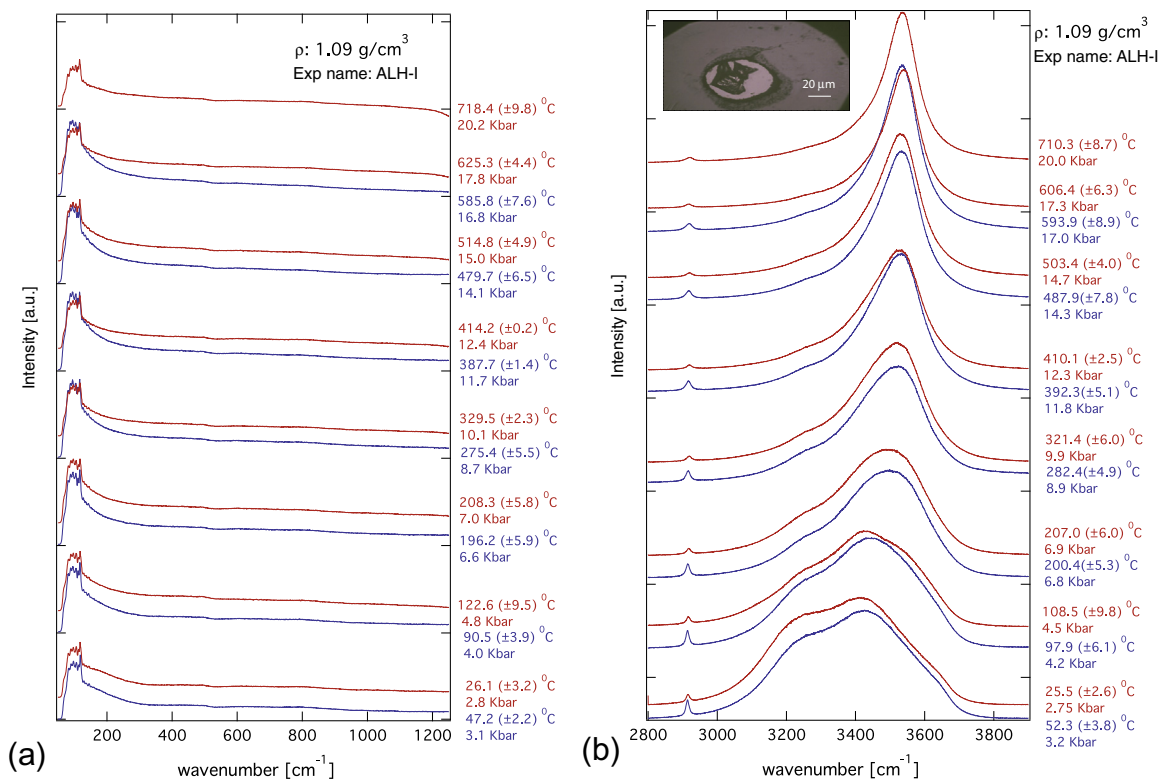
Fig. 4. Raman spectra of pure $H_2O$ in equilibrium with solid corundum as a function of temperature along an isochore with a density of 1.09 g/cm$^3$. (a) shows the spectral region between 100 and 1200 cm$^{-1}$ and (b) shows the spectral region between 2800 and 4000 cm$^{-1}$. The inset shows the gasket and the sample chamber. Within the sample chamber, there is a piece of corundum and vapor bubble is absent. The pressure and the density of the isochore was determined using the shift between the ruby fluorescence at ambient condition and the fluorescence from the corundum piece within the hydrothermal diamond anvil cell. The band owing to the aluminate monomeric species- $[Al(OH)_4]^{1-}$ stretching mode at $\sim$620 cm$^{-1}$ is absent. Also, there is no evidence for dimers and trimer- $[(OH)_3\text{-Al-O-Al-}(OH)_3]^{2-}$, $[(OH)_2\text{-Al-}(OH)_2\text{-Al-}(OH)_2]$, and $[\{-(OH)_2\text{-Al-O-}\}_3]$. The spectra between 2700 and 4000 cm$^{-1}$ shows the bands due to intramolecular $H_2O$. Spectra measured during heating are shown in red, those measured during cooling in blue. Note that the band due to methane ($CH_4$) at 2915 cm$^{-1}$ (Chou and Anderson, 2009) is present in Raman spectra collected at both heating and cooling cycle. This is because the cell underwent several cycles of heating and cooling prior to the Raman measurements. (For interpretation of the references to color in this figure legend, the reader is referred to the web version of this article.)

(Fig. 2). In the blank experiment with pure water, we do see evidence for the interaction of diamond and aqueous fluids at higher temperature with the formation of a band at 2913 cm$^{-1}$ (Fig. 2b). This is likely related to the presence of methane ($CH_4$), as documented by bands at 2918 cm$^{-1}$ (Chou and Anderson, 2009). The band at 2913 cm$^{-1}$ is typically observed in the Raman Spectra collected during the cooling (Fig. 2b). However, this band could also be seen for the Raman spectra collected during the heating paths, if the cell was subjected to repeated heating and cooling prior to the Raman measurements.

The spectral region between 2700 and 4000 cm$^{-1}$ of pure water near ambient conditions is dominated by the vibrations related to $H_2O$ and consisted of three distinct bands at 3256 cm$^{-1}$ ($2v_2$, overtone of bending mode), 3452 cm$^{-1}$ ($v_1$, symmetric stretch) and 3606 cm$^{-1}$ ($v_3$, asymmetric stretch) (Fig. 3). These three bands are very similar to the bands previously reported for pure water- 3225 cm$^{-1}$, 3450 cm$^{-1}$, and 3630 cm$^{-1}$ (Walrafen, 1964). At a temperature of $\sim$696 °C and 8.6 kbar, these bands shift to 3265, 3518, and 3544 cm$^{-1}$, respectively. For the 5.3 m KOH aqueous solution near ambient conditions, the spectral region

between the wavenumber 2700 and 4000 cm$^{-1}$ is characterized by three distinct bands, which occur at 3023 cm$^{-1}$, 3304 cm$^{-1}$, and 3497 cm$^{-1}$. At high temperatures of $\sim$813 °C, 2.2 kbar, these bands shift to 3348, 3542, and 3564 cm$^{-1}$ respectively (Fig. 3). In addition, a sharp feature at 3614 cm$^{-1}$ is also observed for the 5.3 m KOH solution. It is likely due to the excess hydroxyl groups from the dissolved KOH. It could be attributed to a free or "quasifree" (OH$^-$) group i.e., a proton that is not hydrogen bonded (Busing and Hornig, 1961). This band is also attributed to the H–O$\cdots$H–O–H interactions, i.e., $H_2O_2^{1-}$ ions (Walrafen and Douglas, 2006). The oxygen of the hydroxyl group is hydrogen bonded to the other water molecules but the proton attached to the hydroxyl could remains isolated and therefore has a high stretching frequencies as explained from theoretical studies (Hermansson et al., 2011).

In the region 100–1200 cm$^{-1}$, the "pure water" blank experiment is devoid of any vibrational bands. In 5.3 m KOH blank experiment, a vibrational band is identified at 1068 cm$^{-1}$ (full width at half maximum, FWHM $\sim$ 6 cm$^{-1}$). This is likely related to the in-plane deformation of hydroxyl group attached to a water molecule, which causes the sharp

3614 cm$^{-1}$ band. At high temperatures, the vibrational band shifts to lower wavenumbers at 1043 cm$^{-1}$ (FWHM ~ 17 cm$^{-1}$). Close inspection of Fig. 2(c) reveals a very weak band at 935 cm$^{-1}$ at ambient conditions, which shifts to 916 cm$^{-1}$ at 812 °C and 2.2 kbar. This band could be (a) the out-of-plane bending vibration of the same OH$_2$···OH species that causes the 3614 and 1068 cm$^{-1}$ bands; (b) alternatively, it could be the bending vibration of a different OH group. Possibility (a) would be consistent with the empirical observation that the out-of-plane bending vibration usually occurs at considerably lower energies than the in-plane bending vibration (Ryskin, 1974). There is generally an anti-correlation between the frequencies of OH bending and stretching vibrations (Novak, 1974), i.e., if the 935 cm$^{-1}$ band were due to a separate OH species, it should correspond to a stretching vibration with a frequency even higher than that of the 3614 cm$^{-1}$ band. No such vibration is observed, which again makes interpretation (a) more likely.

## 3.2. Al$_2$O$_3$–H$_2$O system

Raman spectra of pure water in equilibrium with corundum were recorded at various temperatures along a high-density isochore (~1.09 g/cm$^3$) (Fig. 4). Solubility of Al$_2$O$_3$ in pure H$_2$O at low pressure and temperatures is low and below the detection limit of the Raman spectrometer, hence the spectra in the region of 100–1200 cm$^{-1}$ are devoid of any features (Fig. 4). We estimate that the detection capabilities of the Raman spectrometer is for solubilities greater than 2.70 ± 0.15 millimolal based on the estimated concentration of alumina (Tropper and Manning, 2007) at pressure temperatures conditions of 700 °C, and ~20 kbar (Fig. 4a). In particular, there is no peak at ~620 cm$^{-1}$, the symmetric stretching mode of [Al(OH)$_4$]$^{1-}$. The vibrational bands at 438 cm$^{-1}$ (the symmetric stretching mode for Al–OH$_2$) (Tossell, 1999) and the bending modes at 656 cm$^{-1}$ due to Al(OH)$_3$·H$_2$O are also missing. The absence of these features indicates that monomeric aluminate species are below detection limit (Fig. 4). Our observation is consistent with a previous study on the Al$_2$O$_3$–H$_2$O system, where monomers were not detected (Davis, 2005).

In the *in situ* studies with corundum in equilibrium with pure water, the spectral region between wavenumber 2700 and 4000 cm$^{-1}$ is unaffected and is dominated by the vibrations related to H$_2$O (Fig. 4). The vibrations related to H$_2$O are characterized by three distinct peaks ($v_1$, 2$v_2$, and $v_3$), which vary as a function of temperature and density (Fig. 5) as shown in Eq. (1).

$$v_i = v_i^0 + \frac{\partial v_i}{\partial T}(T - T_0) + \frac{\partial^2 v_i}{\partial T^2}(T - T_0)^2 + \frac{\partial v_i}{\partial \rho}(\rho - \rho_0)$$
$$+ \frac{\partial^2 v_i}{\partial \rho \partial T}(T - T_0)(\rho - \rho_0) \qquad (1)$$

where, subscript "$i$" refers to 1, 2, and 3 for the three vibrational bands; $v_i^0$ refers to a reference frequency at temperature ($T_0$) and density ($\rho_0$). A least square regression analysis of the data from the Al$_2$O$_3$–H$_2$O system and from the pure H$_2$O system along two different isochores with $\rho = 0.89$ and 1.09 g/cm$^3$ indicates that the band $v_2$ increases with both

temperature and density, with $\frac{\partial v_2}{\partial T} \sim 0.35$ cm$^{-1}$/°C and $\frac{\partial v_2}{\partial \rho} \sim 9.4$ cm$^2$/g, respectively. In contrast to the band $v_2$, the band $v_1$ remains insensitive to temperature and decreases upon compression. The band $v_3$ decreases with both temperature and under compression (Fig. 5). The results of the regression are listed in Table 3.

## 3.3. Al$_2$O$_3$–KOH–H$_2$O system

Raman spectra of 5.3 m KOH solution in equilibrium with corundum up to 800 °C and 7.2 kbar along an isochore with equivalent density of ~0.79 g/cm$^3$ are shown in Fig. 6. The dominant spectral feature between 200 and 1200 cm$^{-1}$ is the 620 cm$^{-1}$ mode. This is attributed to the symmetric stretching mode of [Al(OH)$_4$]$^{1-}$ based on previous Raman spectroscopic studies at low pressure and temperature (620–625 cm$^{-1}$) (Moolenaar et al., 1970;
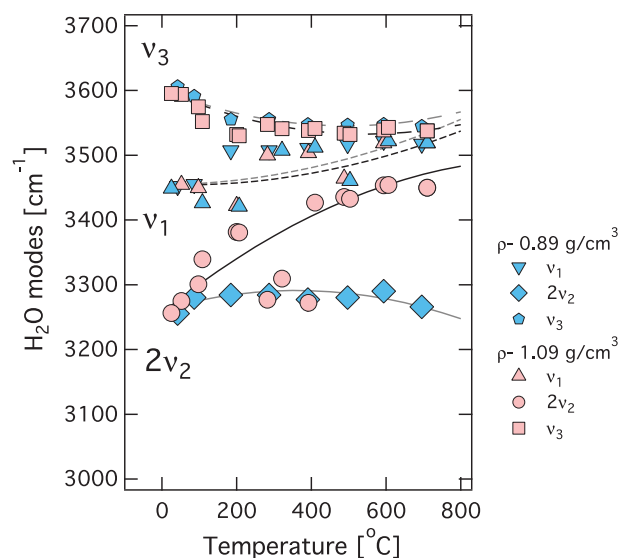


Fig. 5. Temperature dependence of the intramolecular H$_2$O bands 2$v_2$ (overtone of bending mode), $v_1$ (symmetric stretch), and $v_3$ (asymmetric stretch) for two different isochores with densities of 1.09 and 0.89 g/cm$^3$. The overtone of the bending mode is relatively softer and has a large temperature and pressure dependence. The symmetric and asymmetric stretching modes are rather insensitive to pressure and temperature. The fit parameters from the regression are listed in Table 3.

Table 3
Regression parameters for pressure and temperature dependence of the frequencies of the intramolecular bands of H$_2$O, fitted to Eq. (1).

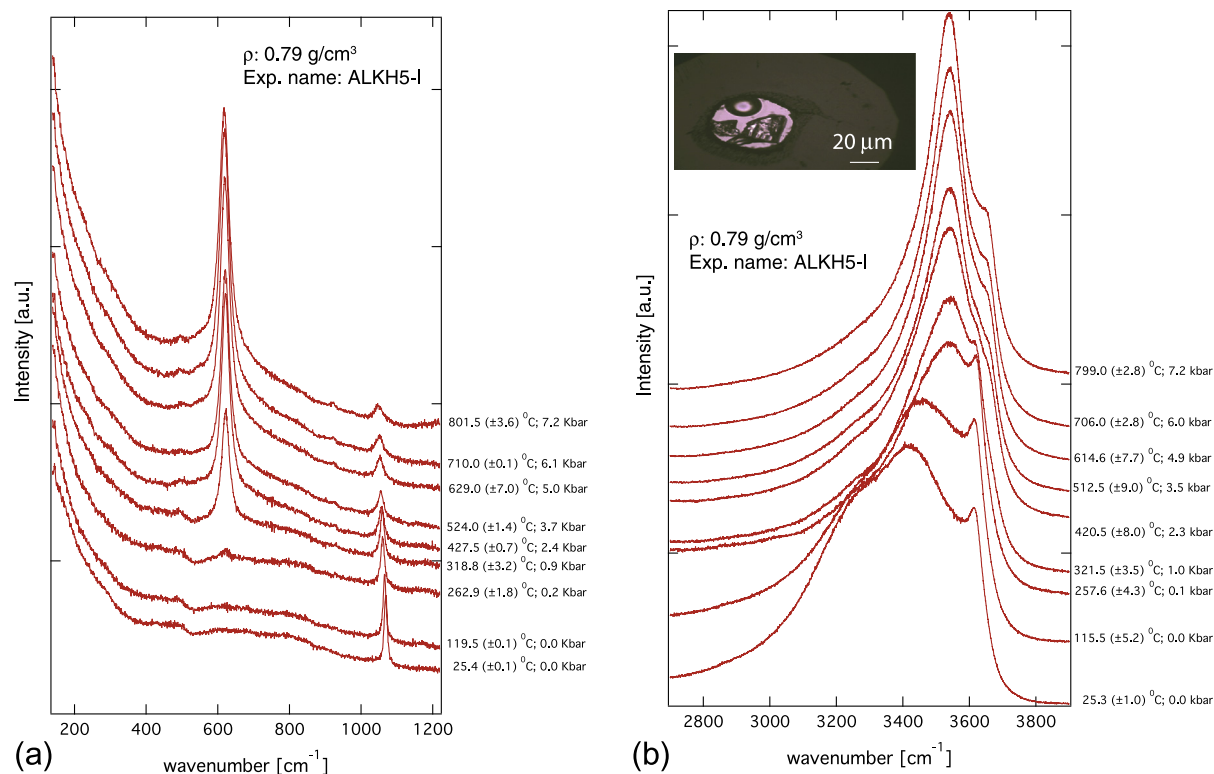|  | $v_1$ | 2$v_2$ | $v_3$ |
|---|---|---|---|
| $v_0$ (cm$^{-1}$) | 3454.1 | 3266.6 | 3595.6 |
| $\partial v_i/\partial T$ (cm$^{-1}$/°C) | 0.00004 | 0.3485 | −0.2316 |
| $\partial v_i^2/\partial T^2$ (cm$^{-1}$/°C)$^2$ | 0.0001 | −0.0002 | 0.0002 |
| $\partial v_i/\partial \rho$ (cm$^{-1}$/g/cm$^3$) | −1.1 | 9.4 | −1.1 |
| $\partial v_i^2/\partial T/\partial \rho$ (cm$^{-1}$/°C/g/cm$^3$) | −0.1 | 1.5 | −0.1 |
| $T_0$ (°C) | 23.4 | 23.4 | 23.4 |
| $\rho_0$ (g/cm$^3$) | 1.0 | 1.0 | 1.0 |

Fig. 6. Raman spectra of 5.3 m KOH fluid in equilibrium with a corundum crystal along an isochore with a nominal density of 0.79 g/cm$^3$. (a) The spectral region from 100 to 1200 cm$^{-1}$ exhibits the main band at ~620 cm$^{-1}$ attributed to the monomer, $[Al(OH)_4]^{1-}$, also seen is the band at ~1068 cm$^{-1}$ due to the deformation mode $\delta(OH)$ from the KOH solution. There is no evidence of polymerized aluminate species. The weak feature near 500 cm$^{-1}$ is due to diamond fluorescence, which was not completely removed by the background correction. (b) The spectral region from 2800 to 4000 cm$^{-1}$, characterizes the intramolecular $H_2O$ bands. Inset shows gasket, sample chamber, corundum crystal and 5.3 m KOH aqueous fluid with a vapor bubble. The spectra were collected along a heating path and are shown in red color. Note the band at 2918 cm$^{-1}$ due to methane ($CH_4$) (Chou and Anderson, 2009) is absent since the Raman spectra were collected during the first cycle. Repeated pressure–temperature cycling of the cell prior to the Raman measurement were avoided. (For interpretation of the references to color in this figure legend, the reader is referred to the web version of this article.)

Watling, 1998; Sipos et al., 2006), as well as our quantum mechanical simulations and previous theoretical studies (Fig. 2; Table 2). The $[Al(OH)_4]^{1-}$ stretching mode appears first at 319 °C and 0.95 kbar respectively and shifts gradually to 618 cm$^{-1}$ upon heating to 800 °C. The integral intensity of the $[Al(OH)_4]^{1-}$ stretching mode also increases with temperature (Fig. 6) due to enhanced alumina solubility in the KOH solution. In the pressure and temperature range explored in the present study (Table 1), we do not find any evidence for polymerization or formation of higher order aluminate species such as dimers -[$(OH)_3$-Al-O-Al$(OH)_3$]$^{2-}$ and [$(OH)_2$-Al-$(OH)_2$-Al$(OH)_2$] or trimers. This is very different from silica, which readily polymerizes at these conditions (Zotov and Keppler, 2002). In experiments with corundum in equilibrium with 1 m KOH solution along a cooling isochore of 0.79 g/cm$^3$, the major feature remains the $[Al(OH)_4]^{1-}$ stretching mode, however, upon cooling the solution is likely supersaturated with the dissolved alumina and the stretching mode remains observable until room temperature. Additional features appear at higher wavenumbers that are likely related to the deformation modes of OH due to KOH.

According to our *ab initio* simulation (Fig. 1, Table 2), it is difficult to tell whether the $[Al(OH)_4]^{1-}$ ion is isolated in solution or whether it forms an ion pair with $K^+$, as there is only a very slight difference (~5 cm$^{-1}$) in the predicted frequency of the main peak for $[Al(OH)_4]^{1-}$ and K$[Al(OH)_4]$. The evolution of peak position and peak width with temperature along an isochore is continuous, without any obvious indication of ion pairing or dissociation.

The spectral region between 2700 and 4000 cm$^{-1}$ is dominated by the hydroxyl (OH) stretching vibrations related to $H_2O$. In the solution with 5.3 m KOH solution the high frequency stretching vibration of the "quasifree" (OH$^-$) group is more intense (Fig. 6) compared to the 1 m KOH solution (Fig. 7).

In an experiment along a high-density isochore (equivalent density of 1.0 g/cm$^3$), with corundum and 5.3 m KOH solution, we noticed that in addition to the stretching mode at 620 cm$^{-1}$, a broad shoulder appeared at 670 cm$^{-1}$ and shifted as a function of temperature with a stronger temperature dependence (Fig. 8). This could be related to the formation of a neutral Al$(OH)_3 \cdot H_2O$ species (compare Fig. 1) However, the additional band is unlikely to be related to a
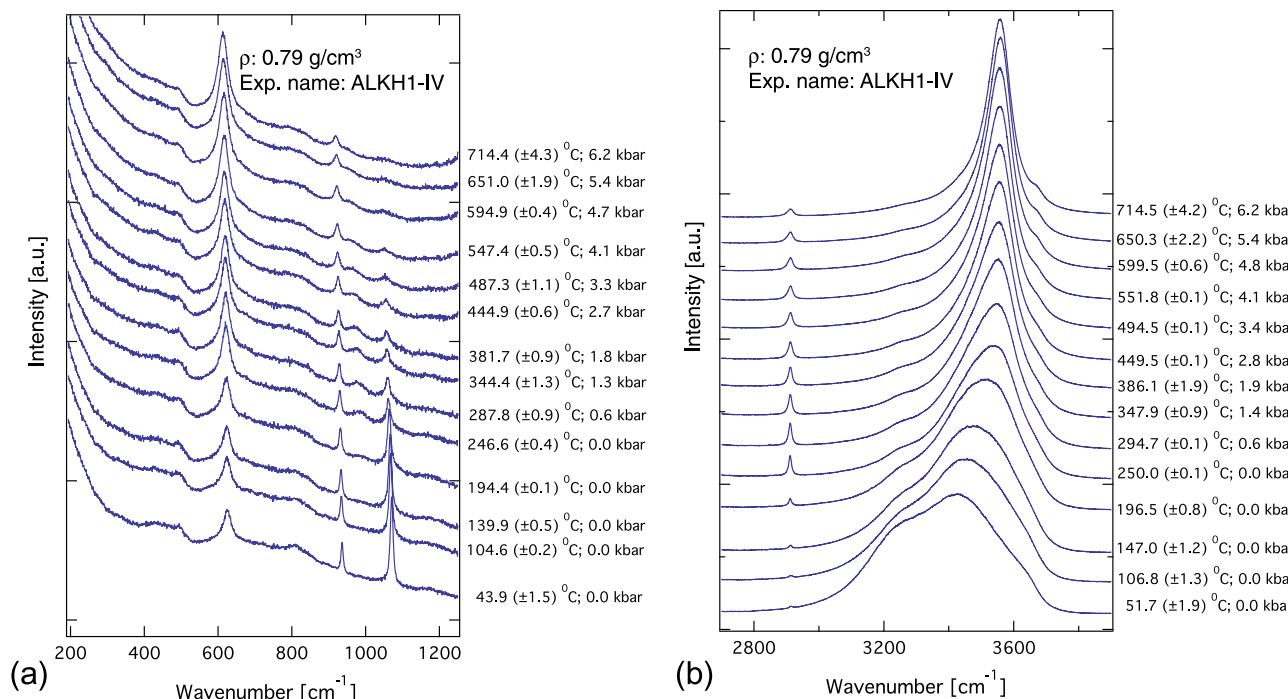
Fig. 7. Raman spectra of 1 m KOH fluid in equilibrium with a corundum crystal measured along a cooling path for an isochore with nominal density of 0.79 g/cm³. (a) The spectral region from 100 to 1200 cm⁻¹ shows the main band at ∼620 cm⁻¹ attributed to the monomer, $[Al(OH)_4]^{1-}$; also seen are the bands at ∼970 cm⁻¹ and 1068 cm⁻¹ due to the deformation mode δ(OH) from the KOH solution. There is no evidence for polymerized aluminate species. Upon cooling, the $[Al(OH)_4]^{1-}$ stretching mode is also seen at room temperature, indicating that the solution is super-saturated. Also observed are features developing at ∼800 cm⁻¹ which are likely due to the precipitation of a thin film of diaspore (AlOOH) in the cooler parts of the sample chamber. (b) The spectral region 2800 and 4000 cm⁻¹ shows the intramolecular $H_2O$ bands.
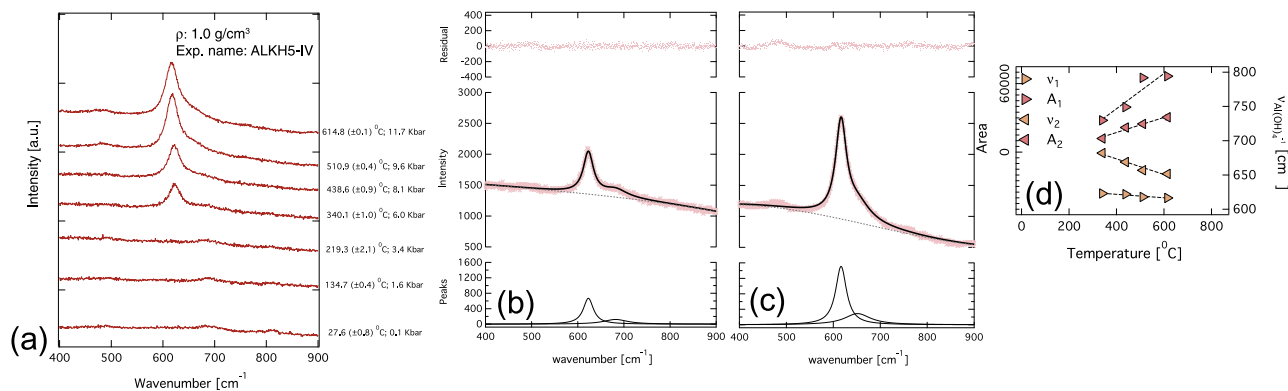


Fig. 8. (a) Raman spectra of 5.3 m KOH fluid in equilibrium with a corundum crystal along an isochore with nominal density of about. 1.0 g/cm³. The spectral region of 400–900 cm⁻¹ is deconvolved into two distinct bands ($v_1$ and $v_2$). There are three panels in (b) and (c), top indicates the residual (pink dots), the middle panel indicates the data (pink crosses), the fit (black line), and the baseline (dashed line) and the lower panel shows the deconvoluted peaks. The bands occur at (b) 623 cm⁻¹ ($v_1$) and 682 cm⁻¹ ($v_2$) at 340 °C, 5.9 kbar, and the bands shift to (c) 617 cm⁻¹ and 652 cm⁻¹ at 614.8 °C, 11.7 kbar. The band at 623 cm⁻¹ is related to the stretching mode of the monomer, $[Al(OH)_4]^{1-}$. The band at higher frequency could be due to $Al(OH)_3·H_2O$ (d) The temperature-induced shift of the monomer peak ($v_1$) and the peak due to $Al(OH)_3·H_2O$ ($v_2$) are −0.03 and −0.11 cm⁻¹/°C respectively. The temperature dependence of the integral intensity of the monomer, $[Al(OH)_4]^{1-}$ ($A_1$) and $Al(OH)_3·H_2O$ ($A_2$) are also shown. (For interpretation of the references to color in this figure legend, the reader is referred to the web version of this article.)

higher order polymer since it co-exists with the monomer at 300 °C. An alternative possibility could be that at higher fluid density the $K[Al(OH)_4]$ species starts to dissociate into $K^+$ and $[Al(OH)_4]^{1-}$, as this may also produce an

additional band on the high-frequency side of the main Raman peak (Fig. 1). This interpretation, however, it not consistent with observations from studies at room temperature (e.g., Watling, 1998; Sipos et al., 2006), where the high
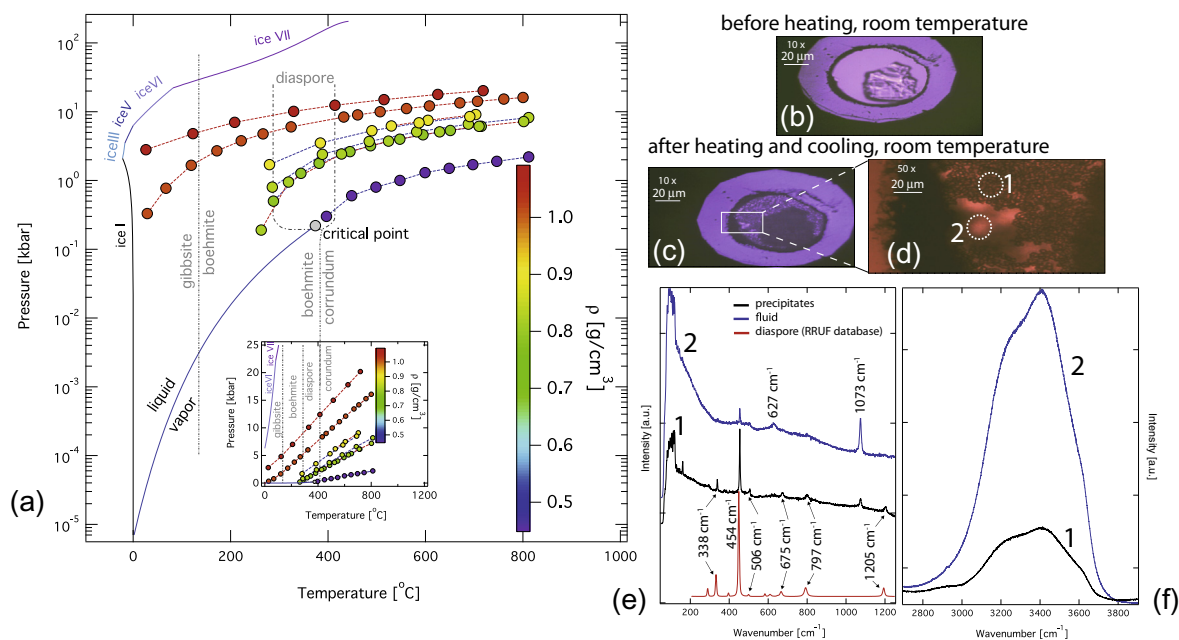
Fig. 9. (a) Phase diagram of $H_2O$. Solid ice phases (I, III, V, VI and VIII) and the liquid $H_2O$ boundary are shown in different shades of blue (Bridgman, 1912; Guildner et al., 1976; IAPWS, 1996; Wagner and Pruß, 2002). The boundary between liquid and vapor phase of $H_2O$ is also shown with the critical point denoted by an grey filled circle. Also shown are the stability fields of various aluminum hydroxide phases (Ervine and Osborn, 1951). As a function of temperature, gibbsite transforms to bohemite and eventually to diaspore. Diaspore is stable until ~400 °C. At temperature greater than 400 °C, corundum is the stable solid. Representative $P$–$T$ paths are shown for experiments from this study. All these paths traverse the aluminum hydroxide stability fields. (b) Gasket and sample chamber, with 1 m KOH solution and a corundum crystal. (c) The corundum crystal has transformed to diaspore. (d) Region 1 – dominated by diaspore (AlOOH), region 2 – dominated by aqueous fluids. (e) The Raman spectra corresponding to region 1 has sharp peaks that correlate with the Raman spectrum for diaspore (natural sample from Turkey, RRUF database- Downs, 2006), Raman spectrum from region 1 has the monomer, $[Al(OH)_4]^{1-}$ mode at 620 cm$^{-1}$, and in addition has sharp features due to formation of diaspore (AlOOH). (f) The intensity of the intramolecular bands are greatly reduced when thin films of diaspore are formed in the cooler region of the sample chamber. (For interpretation of the references to color in this figure legend, the reader is referred to the web version of this article.)

dielectric constant of water should favor dissociation. Indeed, at room temperature, the nature of the cation in the solution (e.g., $K^+$ or $Na^+$) has very little effect on the main band of $[Al(OH)_4]^{1-}$. The room temperature spectra do not show the shoulder at 670 cm$^{-1}$ and accordingly, it is likely not related to the dissociation of an ion pair, but to another species, possibly $Al(OH)_3 \cdot H_2O$.

### 3.4. Precipitates

Unlike silica, which does not form stable hydroxides at pressures and temperatures conditions relevant for crustal and subduction zone settings, there are several stable hydroxides of alumina (e.g., Ervine and Osborn, 1951; Verdes et al., 1992). The aluminum oxide hydroxide AlOOH, diaspore is stable at least up to 400 °C (Haas, 1972). In many experiments, we noticed additional sharp peaks occurring at 338 cm$^{-1}$, 454 cm$^{-1}$, and 797 cm$^{-1}$ upon cooling of $Al_2O_3$-saturated solutions to room temperature. These bands correspond to diaspore crystals, which apparently precipitated throughout the sample chamber. Raman spectra of the fluid show the $[Al(OH)_4]^{1-}$ stretching mode in addition to some of the vibrational bands of diaspore (Fig. 9).

Table 4
Regression parameters for the pressure and temperature dependence of the frequency and integrated intensity of the $[Al(OH)_4]^{1-}$ stretching mode, fitted to Eqs. (3) and (4).

|  | 5.3 m KOH | 1 m KOH |
|---|---|---|
| $v_0$ (cm$^{-1}$) | 623.62 | 621.70 |
| $\partial v_{[Al(OH)_4]^{1-}}/\partial T$ (cm$^{-1}$/°C) | −0.01 | −0.02 |
| $\partial v_{[Al(OH)_4]^{1-}}/\partial \rho$ (cm$^{-1}$/g/cm$^3$) | 15.72 | 17.85 |
| $A_0$ (cm$^{-1}$) | 4.6e−08 | 3.3e−08 |
| $\partial A_{[Al(OH)_4]^{1-}}/\partial T$ (cm$^{-1}$/°C) | 7260.91 | 5193.10 |
| $\partial A_{[Al(OH)_4]^{1-}}/\partial \rho$ (cm$^{-1}$/g/cm$^3$) | −2769585.65 | −4823193.43 |
| $T_0$ (°C) | 25.00 | 24.23 |
| $\rho_0$ (g/cm$^3$) | 0.66 | 0.82 |

### 4. DISCUSSION

The similarity of the Raman spectra obtained from the experiments conducted at different bulk densities in KOH–$H_2O$ aqueous solution indicates that apart from the anharmonic effects, the $[Al(OH)_4]^{1-}$ molecule exists as a well defined entity without significant distribution of bond length, bond angles and polarizability parameters. The relatively high concentration of this anionic species is

consistent with the alkaline conditions (Wohlers and Manning, 2009). In experiments with high fluid density, we have observed bands that might be attributed to $Al(OH)_3 \cdot H_2O$.

The concentration of $[Al(OH)_4]^{1-}$ in $KOH-H_2O$ solutions should be directly proportional to the integral intensity of the $\sim 620$ cm$^{-1}$ band. The integral intensities were calculated for the monomer peak at $\sim 620$ cm$^{-1}$ and were corrected for thermal effects by the thermal population factor, $R$ (Zotov and Keppler, 2002)

$$R = v\left(1 - \exp\left(-\frac{hcv}{k_B T}\right)\right) \qquad (2)$$

where, $v$ is the frequency, $h$ is the Planck's constant, $c$ is the speed of light, $k_B$ is the Boltzman constant and $T$ is the absolute temperature in Kelvin.

In the *in situ* studies with corundum in equilibrium with 5.3 m KOH and 1 m KOH solutions, the variation of the frequency and integral intensity of the $[Al(OH)_4]^{1-}$ stretching band can be described by the equations

$$v_{[Al(OH)_4]^{1-}} = v_0 + \frac{\partial v_{[Al(OH)_4]^{1-}}}{\partial T}(T - T_0) + \frac{\partial v_{[Al(OH)_4]^{1-}}}{\partial \rho}(\rho - \rho_0) \qquad (3)$$

and,

$$A_{[Al(OH)_4]^{1-}} = A_0 + \frac{\partial A_{[Al(OH)_4]^{1-}}}{\partial T}(T - T_0) + \frac{\partial A_{[Al(OH)_4]^{1-}}}{\partial \rho}(\rho - \rho_0) \qquad (4)$$

The thermally corrected integral intensities were converted to concentrations (mol/kg of $H_2O$) units using the reported alumina solubility in 1 m KOH solution as calibration point (Wohlers and Manning, 2009). We calibrate the intensity of the monomer as

$$C_{[Al(OH)_4]^{1-}} = k_{[Al(OH)_4]^{1-}} \times A_{[Al(OH)_4]^{1-}} \qquad (5)$$

where, the concentration of the monomer, $C_{[Al(OH)_4]^{1-}}$ is from the solution experiments (Wohlers and Manning, 2009), the intensity of the monomer, $A_{[Al(OH)_4]^{1-}}$ is derived from the *in situ* experiments and the integral intensity of the 620 cm$^{-1}$ bands (Fig. 10) and $k_{[Al(OH)_4]^{1-}}$ contains the scattering cross section at various instrument parameters. We used $k_{[Al(OH)_4]^{1-}}$ and the intensity of the monomer for a range of isochores and with varying temperatures to predict the monomer concentrations, which should be equivalent to bulk alumina solubilities in these alkaline solutions. Results are shown in Fig. 10 (see Table 4 for the regression parameters).

## 5. CONCLUSION

This study demonstrates that *in situ* Raman Spectroscopy in externally heated diamond anvil-cells allows identification of the major aluminate species dissolved in alkaline aqueous solution with 5.3 m and 1 m KOH solution in equilibrium with corundum. The dominant species is the monomer $[Al(OH)_4]^{1-}$ species at all temperatures greater than $\sim 300$ °C. Within the temperature, pressure, and density explored in the present study, there is no evidence for polymerization via formation of e.g., $[(OH)_2\text{-}Al\text{-}(OH)_2\text{-}Al(OH)_2]$ dimer species. In pure $H_2O$, the monomer species is beyond the detection limit of the Raman spectrometer as the solubility of corundum is very low. Our data therefore show that for typical crustal $P$, $T$ conditions, thermodynamic models of alumina in aqueous solutions may safely ignore polymerization effects, in particular when the bulk alumina solubilities are low. This does not, however, rule out the potential importance of polymeric species at deeper mantle with $P$ (>20 kbar), $T$ (>1000 °C) conditions where higher bulk alumina solubilities may enhance polymerization.


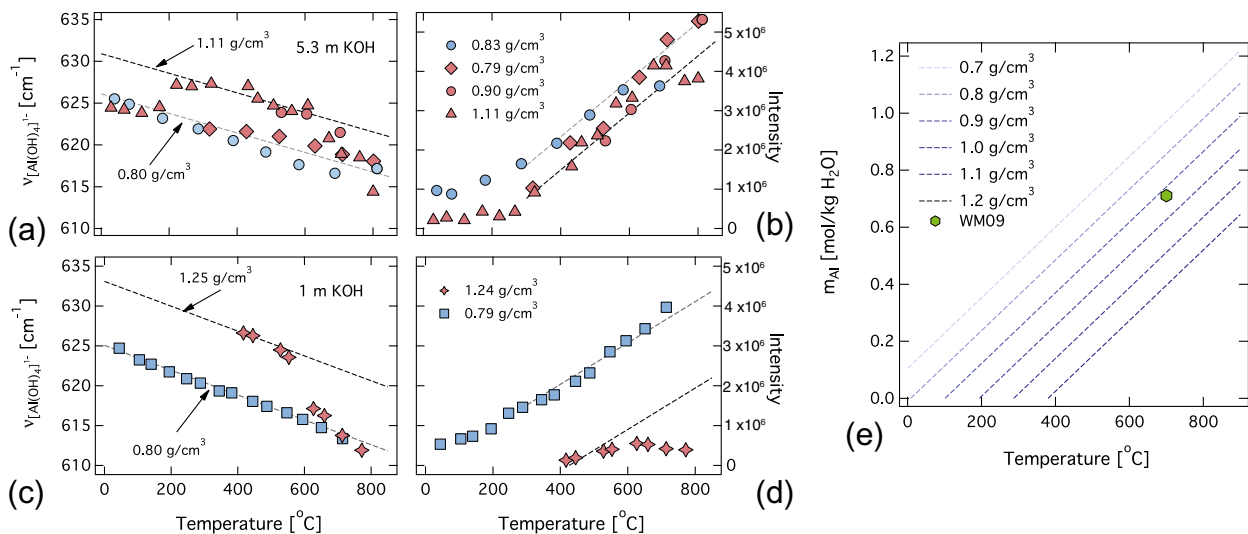
Fig. 10. Dependence of frequency and intensity of the $[Al(OH)_4]^{1-}$ stretching mode on temperature and density for (a, b) 5.3 m KOH aqueous solution and (c, d) 1 m KOH solution. The integral intensities were corrected with the thermal population factor (Eq. (2), see text). The deviation of the data for the 1.25 g/cm$^3$ isochore from the initial trend are likely due to a leak of the sample chamber (e) Variation of Al concentration in 1 m KOH in equilibrium with corundum as a function of temperature and density. Data below 400 °C represent metastable equilibria.

## REFERENCES

Anderson G. M. (1995) Is there alkali–aluminum complexing at high temperatures and pressures? *Geochim. Cosmochim. Acta* **59**, 2155–2161.

Anderson G. M. and Burnham C. W. (1967) Reactions of quartz and corundum with aqueous chloride and hydroxide solutions at high temperatures and pressures. *Am. J. Sci.* **265**, 12–27.

Anderson G. M. and Burnham C. W. (1983) Feldspar solubility and the transport of aluminum under metamorphic conditions. *Am. J. Sci.* **283-A**, 283–297.

Azaroual M., Pascal M. L. and Roux J. (1996) Corundum solubility and aluminum speciation in KOH aqueous solutions at 400 °C from 0.5 to 2.0 kbar. *Geochim. Cosmochim. Acta* **60**, 4601–4614.

Barns R. L., Shields R. M. and Laudise R. A. (1963) Solubility of corundum in basic hydrothermal solvents. *J. Phys. Chem.* **67**, 835.

Bassett W. A. (2003) High pressure–temperature aqueous systems in the hydrothermal diamond anvil cell (HDAC). *Eur. J. Mineral.* **15**, 773–780.

Bassett W. A., Shen A. H., Bucknum M. and Chou I. M. (1993a) A new diamond-anvil cell for hydrothermal studies to 2.5 GPa and from −190 °C to 1200 °C. *Rev. Sci. Inst.* **64**, 2340–2345.

Bassett W. A., Shen A. H., Bucknum M. and Chou I. M. (1993b) Hydrothermal studies in a new diamond anvil cell up to 10 GPa and from −190 °C to 1200 °C. *Pure Appl. Geophys.* **141**, 487–495.

Becke A. D. (1993) Density-functional thermochemistry. III. The role of exact exchange. *J. Chem. Phys.* **98**, 5648–5652.

Bridgman P. W. (1912) Water, in the liquid and five solid forms, under pressure. *Proc. Am. Acad. Arts Sci.* **47**, 439–558.

Busing W. R. and Hornig D. F. (1961) The effect of dissolved KBr, KOH, or HCl on the Raman spectrum of water. *J. Chem. Phys.* **65**, 284–292.

Casey W. H. (2005) Large aqueous aluminum hydroxide molecules. *Chem. Rev.* **106**, 1–16.

Casey W. H. and Rustad J. R. (2007) Reaction dynamics, molecular clusters, and aqueous geochemistry. *Annu. Rev. Earth Planet. Sci.* **35**, 21–46.

Chellappa R. S., Somayazulu M. and Hemley R. J. (2009) Rhenium reactivity in $H_2O$–$O_2$ supercritical mixtures at high pressures. *High Press. Res.* **29**, 792–799.

Chou I.-M. and Anderson A. J. (2009) Diamond dissolution and the production of methane and other carbon-bearing species in hydrothermal diamond-anvil cells. *Geochim. Cosmochim. Acta* **73**, 6360–6366.

Davis M. K. (2005). Fluid rock interactions in silicate and aluminosilicate systems at elevated pressure and temperature. Doctoral dissertation, Retrieved from ProQuest Dissertations and Theses, Univ. Michigan, AAT3186610.

Diakonov I., Pokrovski G., Schott J., Castet S. and Gout R. (1996) An experimental and computational study of sodium–aluminum complexing in crustal fluids. *Geochim. Cosmochim. Acta* **60**, 197–211.

Downs R. T. (2006). The RRUF Project: an integrated study of the chemistry, crystallography, Raman and infrared spectroscopy of minerals. Program. Abstracts. 19th General Meeting of the Int. Min. Assoc., Kobe, Japan, O 03-13.

Ervine G. and Osborn E. F. (1951) The system $Al_2O_3$–$H_2O$. *J. Geol.* **59**, 381–394.

Frisch M.J., et al. (2009). Gaussian 09, Revision, A. 1. Gaussian Inc., Wallingford, CT.

Gale J. D., Rohl A. L., Walting H. R. and Parkinson G. M. (1998) Theoretical investigation of the nature of aluminum-containing species present in alkaline solution. *J. Phys. Chem. B.* **102**, 10372–10382.

Guildner L. A., Johnson D. P. and Jones F. E. (1976) Vapor pressure of water at its triple point. *J. Res. Natl. Bur. Stand.* **80A**, 505–521.

Haas H. (1972) Diaspore–corundum equilibrium determined by epitaxis of diaspora on corundum. *Am. Mineral.* **57**, 1375–1385.

Hehre W., Radom L., Schleyer P. V. R. and Pople J. A. (1986) *Ab Initio Molecular Orbital Theory*. Wiley, New York.

Hermansson K., Bopp P. A., Spangberg D., Pejov L., Bako I. and Mitev P. D. (2011) The vibrating hydroxide ion in water. *Chem. Phys. Lett.* **514**, 1–15.

IAPWS (1996). IAPWS Release on the IAPWS formulation 1995 for the thermodynamic properties of ordinary water substance for general and scientific use. Available at: <http://www.iapws.org>.

Iler R. K. (1979) *The Chemistry of Silica: Solubility, Polymerization, Colloid and Surface Properties and Biochemistry of Silica*. John Wiley and Sons, New York, ISBN: 978-0-471-02404-0, p. 896.

Kerrick D. M. (1990) The $Al_2SiO_5$ polymorphs. *Rev. Mineral.* **22**, 406.

Korzhinskiy M. A. (1987) The solubility of corundum in an HCl fluid and forms taken by Al. *Geochem. Int.* **24**, 105–110.

Lee C., Yang W. and Parr R. G. (1988) Development of the Colle-Salvetti correlation-energy formula into a functional of the electron density. *Phys. Rev. B.* **37**, 785–789.

Manning C. E. (1994) The solubility of quartz in the lower crust and upper mantle. *Geochim. Cosmochim. Acta* **58**, 4831–4839.

Manning C. E. (2007) Solubility of corundum + kyanite in H2O at 700 °C, 10 kbar: evidence for Al–Si complexing at high pressure and temperature. *Geofluids* **7**, 258–269.

Mao H. K., Xu J. and Bell P. M. (1986) Calibration of the ruby pressure gauge to 800 kbar under quasi-hydrostatic conditions. *J. Geophys. Res.* **91**, 4673–4676.

Mibe K., Chou I.-M. and Bassett W. A. (2008) In situ Raman spectroscopic investigation of the structure of subduction-zone fluids. *J. Geophys. Res.* **113**, B04208.

Moolenaar R. J., Evans J. C. and McKeever L. D. (1970) The structure of aluminate ion I solutions at high pH. *J. Phys. Chem.* **74**, 3629–3636.

Newton R. C. and Manning C. E. (2002) Solubility of silica in equilibrium with enstatite, forsterite, and $H_2O$ at deep crust/upper mantle pressures and temperatures and an activity-concentration model for polymerization of aqueous silica. *Geochim. Cosmochim. Acta* **66**, 4165–4176.

Newton R. C. and Manning C. E. (2003) Activity coefficient and polymerization of aqueous silica at 800 °C, 12 kbar, from solubility measurements on $SiO_2$-buffering mineral assemblages. *Contrib. Mineral. Pet.* **146**, 135–143.

Newton R. C. and Manning C. E. (2006) Solubilities of corundum, wollastonite and quartz in $H_2O$–NaCl solutions at 800 °C and 10 kbar: interaction of simple minerals with brines at high pressure and temperature. *Geochim. Cosmochim. Acta* **70**, 5571–5582.

Novak A. (1974) Hydrogen bonding in solids. Correlation of spectroscopic and crystallographic data. *Struct. Bond.* **18**, 177–216.

Pascal M. L. and Anderson G. M. (1989) Speciation of Al, Si, and K in supercritical solutions: experimental study and interpretation. *Geochim. Cosmochim. Acta* **53**, 1843–1855.

Pokrovskii G. S., Schott J., Harrichoury J. C. and Sergeyev A. S. (1996) The stability of aluminum silicate complexes in acidic solutions from 25–150 °C. *Geochim. Cosmochim. Acta* **60**, 2495–2501.

Pokrovskii V. A. and Helgeson H. C. (1995) Thermodynamic properties of aqueous species and the solubilities of minerals at high pressures and temperatures: the system $Al_2O_3$–$H_2O$–NaCl. *Am. J. Sci.* **295**, 1255–1342.

Pokrovskii V. A. and Helgeson H. C. (1997) Thermodynamic properties of aqueous species and the solubilities of minerals at high pressures and temperatures: the system $Al_2O_3$–$H_2O$–KOH. *Chem. Geol.* **137**, 221–242.

Pople J. A., Scott A. P., Wong M. W. and Radom L. (1993) Scaling factors for obtaining fundamental vibrational frequencies and zero-point energies from HF/6-31G* and MP2/6-31G* harmonic frequencies. *Israel J. Chem.* **33**, 345–350.

Ragnarsdottir K. V. and Walther J. V. (1985) Experimental determination of corundum solubilities in pure water between 400–700 °C and 1–3 Kbar. *Geochim. Cosmochim. Acta* **49**, 2109–2115.

Ryskin Y. A. (1974) The vibrations of protons in minerals: hydroxyl, water and ammonium. In *The infrared spectra of minerals* (ed. V. C. Farmer). Mineralogical Society, London, pp. 137–181.

Sanjuan B. and Michard G. (1987) Aluminum hydroxide solubility in aqueous solutions containing fluoride ions at 50 °C. *Geochim. Cosmochim. Acta* **51**, 1823–1831.

Salvi S., Pokrovski G. S. and Shott J. (1998) Experimental investigation of aluminum-silica aqueous complexing at 300 °C. *Chem. Geol.* **151**, 51–67.

Saul A. and Wagner W. (1989) A fundamental equation for water covering the range from the melting line to 1273 K at pressures up to 25000 MPa. *J. Phys. Chem. Ref. Data* **18**, 1537–1559.

Sipos P., May P. M. and Hefter G. (2006) Quantitative determination of an aluminate dimer in concentrated alkaline aluminate solutions by Raman spectroscopy. *Dalton Trans.* **2006**, 368–375.

Tagirov B. and Schott J. (2001) Aluminum speciation in crustal fluids revisited. *Geochim. Cosmochim. Acta* **65**, 3965–3992.

Tossell J. A. (1999) Theoretical studies on aluminate and sodium aluminate species in models for aqueous solution: $Al(OH)_3$, $Al(OH)_4^-$, and $NaAl(OH)_4$. *Am. Mineral.* **84**, 1641–1649.

Tropper P. and Manning C. E. (2007) The solubility of corundum in $H_2O$ at high pressure and temperature and its implications for Al mobility in the deep crust and upper mantle. *Chem. Geol.* **240**, 54–60.

Verdes G., Gout R. and Castet S. (1992) Thermodynmic properties of the aluminate ion and of bayerite, boehmite, diaspora and gibbsite. *Eur. J. Mineral.* **4**, 767–792.

Wagner W. and Pruß A. (2002) The IAPWS formulation 1995 for the thermodynamic properties of ordinary water substance for general and scientific use. *J. Phys. Chem. Ref. Data* **31**, 387–535.

Walrafen G. E. (1964) Raman spectral studies of water structure. *J. Chem. Phys.* **40**, 3249–3256.

Walrafen G. E. and Douglas R. T. W. (2006) Raman spectra from very concentrated aqueous NaOH and from wet and dry, solid, and anhydrous molten. LiOH, NaOH, and KOH. *J. Chem. Phys.* **124**, 114504.

Walther J. V. (1997) Experimental determination and interpretation of the solubility of corundum in $H_2O$ between 350 and 600 °C from 0.5 to 2.2 kbar. *Geochim. Cosmochim. Acta* **61**, 4955–4964.

Walther J. V. (2001) Experimental determination and analysis of the solubility of corundum in 0.1 and 0.5 m NaCl solutions between 400 and 600 °C. *Geochim. Cosmochim. Acta* **65**, 2843–2851.

Watling H. (1998) Spectroscopy of concentrated sodium aluminate solutions. *Appl. Spectrosc.* **52**, 250–258.

Wasserburg G. J. (1958) The solubility of Quartz in supercritical water as a function of pressure. *J. Geol.* **66**, 559–578.

Wei Q., Dubovinskaia N. and Dubrovinsky L. (2011) Ruby and Sm: YAG fluorescence pressure gauges up to 120 GPa and 1700 K. *J. App. Phys.* **110**, 043513.

Wohlers A. and Manning C. E. (2009) Solubility of corundum in aqueous KOH solutions at 700 °C and 1 GPa. *Chem. Geol.* **262**, 310–317.

Zotov N. and Keppler H. (2000) In-situ Raman spectra of dissolved silica species in aqueous fluids to 900 °C and 14 kbar. *Am. Mineral.* **85**, 600–603.

Zotov N. and Keppler H. (2002) Silica speciation in aqueous fluids at high pressures and high temperatures. *Chem. Geol.* **184**, 71–82.

*Associate editor:* Bjorn Jamtveit